DRAFT VERSION APRIL 4, 2016
Preprint typeset using LaTeX style emulateapj v. 12/16/11

FINDING SPLASHBACK RADII IN COSMOLOGICAL SIMULATIONS

PHILIP MANSFIELD[1,2,⋆], ANDREY V. KRAVTSOV[1,2,3] AND BENEDIKT DIEMER[4]

Draft version April 4, 2016

ABSTRACT

The splashback radius is a drop in the outer density profile of dark matter halos caused by particles on the apocenters of their first orbit. This feature has recently gained interest as a physically motivated halo boundary. However, up to this point all analysis of the splashback radius has been done on stacked, radially averaged profiles which fail to account for the large variance and asphericity of this feature. In this paper we present the code Shellfish (SHELL Finding In Spheroidal Halos) which can identify the full 3D shape of these shells quickly for individual halos from a single particle snapshot.

Subject headings: cosmology: theory – dark matter – methods: numerical

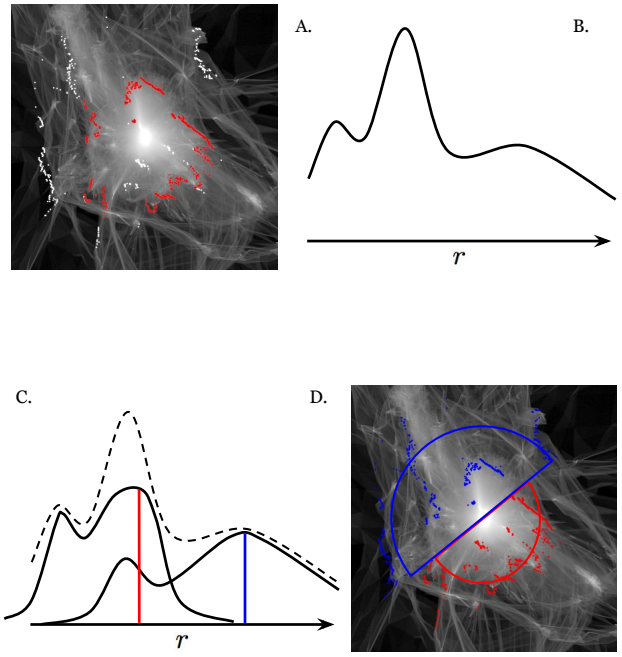

FIG. 1.— An illustration of Shellfish's filtering algorithm. Panel A shows a slice through the density field of a halo with the points of steepest slope along 1024 uniformly spaced lines of sight shown as red and white dots. For this halo, there are three populations of dots: those which correspond to the splashback shell (roughly shown in red), those which correspond to subhalos within the splashback shell and those which correspond to filaments outside the splashback shell. A cartoon representing the distribution of radii is shown in panel B. **TODO: Flip C and D, make less ugly. Make caption shorter.**

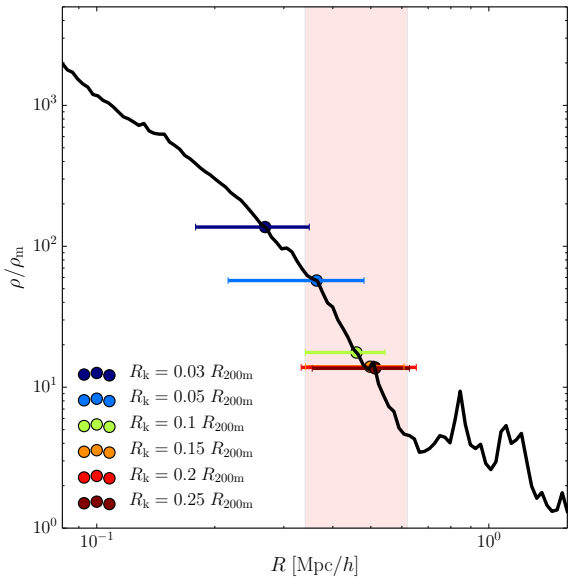

FIG. 2.— Convergence test of $R_{\rm sp}$ as a function of kernel radius for a representitive halo. The black curve is the density profile of the halo, the points are the $R_{\rm sp}$ values measured at different kernel radii, the horizonal lines show the range spanned by $R_{\rm min}$ and $R_{\rm min}$ for these shells, and the shaded red region corresponds to the radial range which was visually identified as corresponding to the splashback range. This region was found without knowledge of the measurments made by Shellfish in accordance with the procedure outlined in Appendix B. For this halo, $R_{\rm sp}$ is converged for kernel radii above $0.15R_{\rm k}$

1. INTRODUCTION

Placeholder text.

2. METHODS

Placeholder text.

3. RESULTS

Placeholder text.

4. DISCUSSION

Placeholder text.

5. SUMMARY AND CONCLUSIONS

Placeholder text.

Placeholder text.

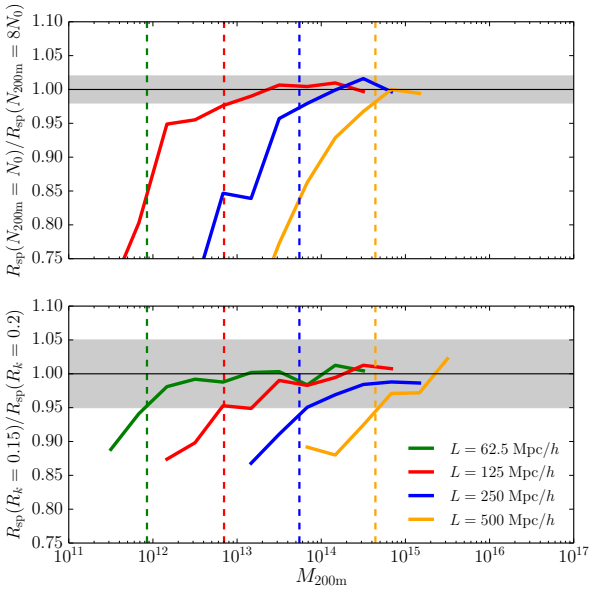

FIG. 3.— Convergence test of $R_{\rm sp}$ with $N_{\rm 200m}$. The top panel shows the median ratio of $R_{\rm sp}$ to the value of $R_{\rm sp}$ that would be measured if that halo was resolved with 8 times the resolution for halos of a given mass in each simulation in our suite. This value is simulated by comparing subsampled and fully sampled halos from a a more finely resolved simulation. The bottom panel shows the median ratio of $R_{\rm sp}$ measured with kernel radii of $R_{\rm k} = 0.15 \times R_{\rm 200m}$ to $R_{\rm sp}$ measured with kernel radii of $R_{\rm k} = 0.20 \times R_{\rm 200m}$. The vertical lines show the masses at which $N_{\rm 200m} = 5 \times 10^4$ in each simulation, and the shaded gray regions show the size of 2% and 5% deviations for the upper and lower panels, respectively. The top panel uses kernel sizes of $R_{\rm k} = 0.20 \times R_{\rm 200m}$. The top panel demonstrates that a systematic offset of $\gtrsim 2\%$ can be expected at $N_{\rm 200m} < 5 \times 10^4$. The bottom panel demonstrates that the particle counts which correspond to a 2% reduction in radius under subsampling result in a 5% reduction in radius under kernel size reduction. The significance of this alignment is discussed in the text. (**This is likely to be confusing.**)

REFERENCES

Abel, T., Hahn, O., & Kaehler, R. 2012, MNRAS, 427, 61
More, S., Diemer, B., & Kravtsov, A. V. 2015, ApJ, 810, 36
Powell, D., & Abel, T. 2014, ArXiv e-prints

APPENDIX

A. AN ALGORITHM FOR FAST LOS DENSITY MEASUREMENTS

The first step of Shellfish's shell-finding algorithm is to assign densities to a large number of lines of sight anchored the center of each halo. In the case where density estimates are constructed by converting particles into a set of volume-filling constant density convex solids (such as spherical top hat kernels or constant density tetrahedra under the method of Abel et al. 2012), the density along a line of sight, l, is

$$\rho_l(r) = \sum_{i=0}^{i<N} \mathbb{I}_{\rm intr} \rho_i H(r - r_{\rm in}) H(r_{\rm out} - r), \tag{A1}$$

where i indexes over all the solid, $\mathbb{I}_{\rm intr}$ is an indicator function which is 1 if the solid intersects with solid i and 0 otherwise, ρ_i is the density of this solid, H is the Heaviside step function, and $r_{\rm in}$ and $r_{\rm out}$ are the distances to entrance and exit intersection points, respectively.

For a typical choice of density estimator the number of zero terms in Eq. A1 dwarfs the number of non-zero terms, making efficient evaluation of $\mathbb{I}_{\rm intr}$ critical. This is trivial if a density estimate is written to an intermediate grid before being translated onto the lines of sight, since the grid cell that corresponds to the point at radius r of given ray can be calculated in $O(1)$. However, using an intermediate grid has a number of disadvantages:

[1] Department of Astronomy & Astrophysics, The University of Chicago, Chicago, IL 60637 USA
[2] Kavli Institute for Cosmological Physics, The University of Chicago, Chicago, IL 60637 USA
[3] Enrico Fermi Institute, The University of Chicago, Chicago, IL 60637 USA
[4] Institute for Theory and Computation, Harvard-Smithsonian Center for Astrophysics, 60 Garden St., Cambridge, MA 02138, USA
* mansfield@uchicago.edu

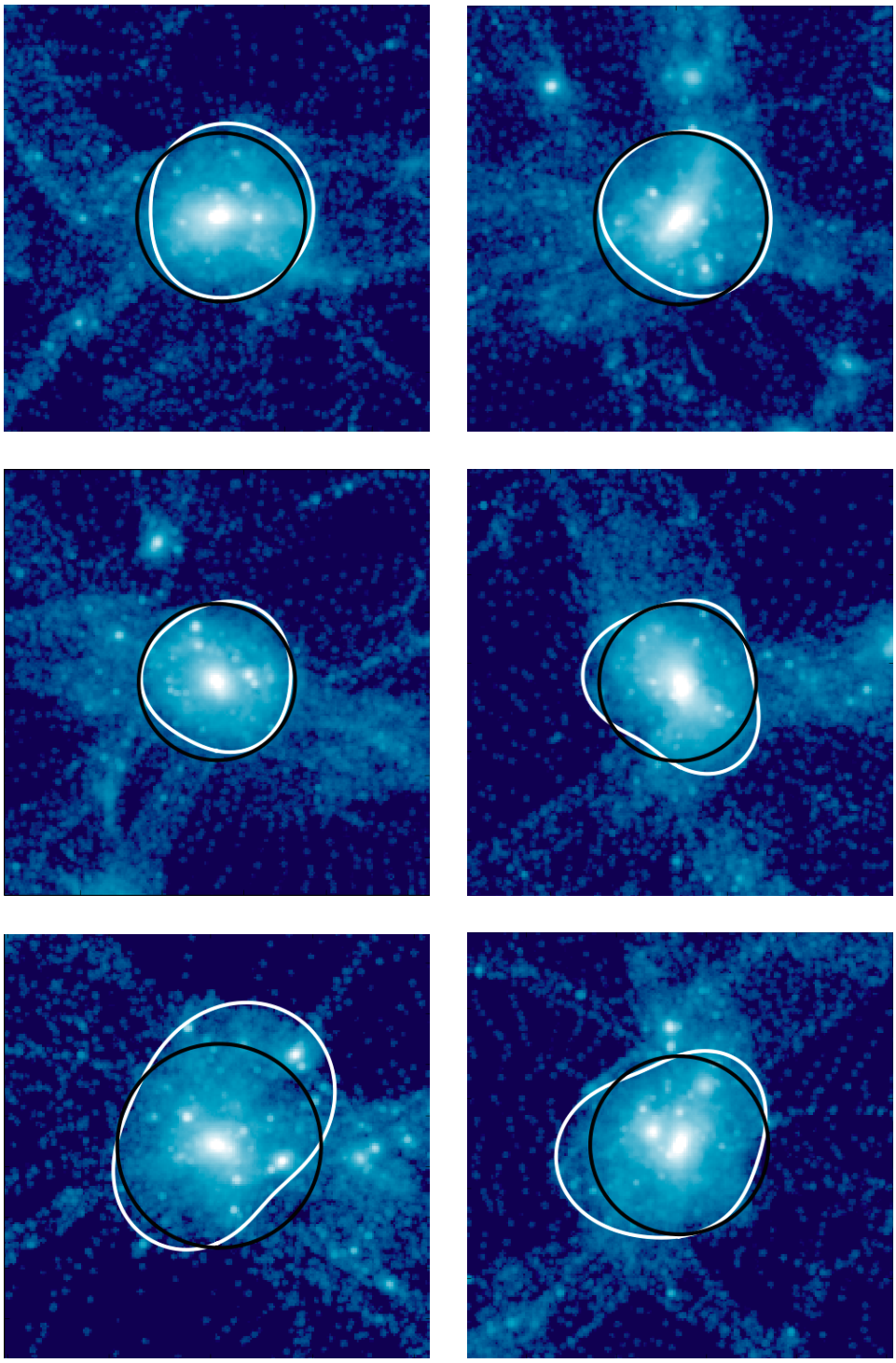

FIG. 4.— Density slices of six randomly selected halos compared to the shells measured by Shellfish. The shape of the shell within this slice is shown by the white curve and the a sphere with the same volume as the shell is shown in black. The six halos were picked uniformly from the $\log M_{200\mathrm{m}} - \log \Gamma$ plane in out `L0063` simulation box and are each plotted out to $2.5R_{200\mathrm{m}}$.

1. Maintaining the high-resolution grid required to measure asphericities in the splashback shell consumes a large amount of space. This restricts the number of halos which can be maintained in memory at once. In the case where a user requests analysis of more halos than can fit memory at once, Shellfish would need to read particle catalogs from disk multiple times.

2. Writing the density esitmate to a grid is expensive as it involves either an exact raterization scheme (see, for example, Powell & Abel 2014) or Monte Carlo sampling of each solid with sufficiently many points to elimate shot noise in the estimate. This will also require that density estimates are calculated for grid cells which are not intersected by any line of sight.

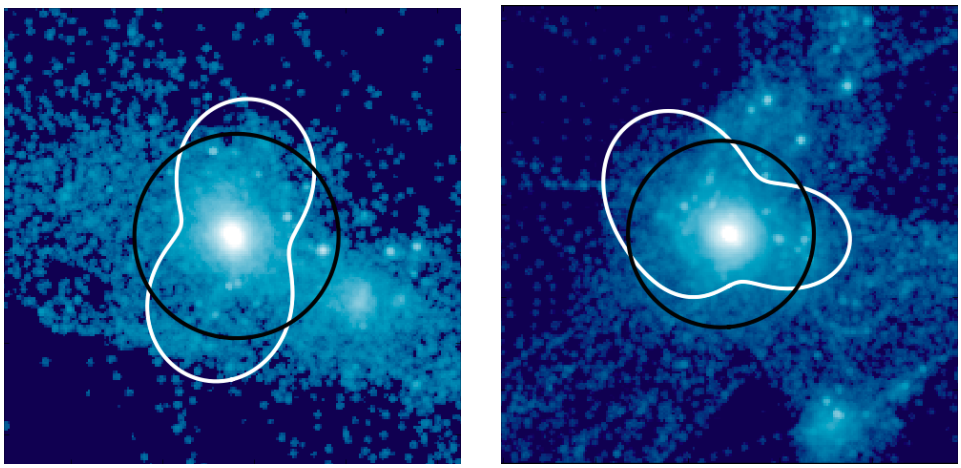

FIG. 5.— Examples of halos for which Shellfish produces poor shells. These halos were chosen by randomly selecting halos from the population of halos which fail the cut described in Appendix until two were found which did not appear to be good fits by eye. The left panel is typical these types of halos: they often inhabit strong filaments and do not contain a visually apparent splashback shell in their dentity fields, although, as demonstrated in the right panel, there are some halos with visually apparent splashback fields which Shellfish measures incorrectly, too. The right panel also demonstrates that even in cases where the full shell is incorrect, the volume-equivalent radius can be relatively well-behaved. We estimate that Shellfish generates these types of shells for roughly 5% of the halos in our sample.

3. Introducing an intermediate grid reduces the fidelity of the line of sight density estimates due to pixelation. This is most apparent as small radii.

In practice we find that these three disadvantages, particularly the second, make the use of grids undesirable for Shellfish. For this reason, we designed an algorithn which evaluates Eq. A1 exactly up to the resolution of the line of sight profiles without the use of a grid.

Preamble goes here. Split up into halos and rings.[6]. For each particle catalog file, the following actions are performed:

1. A bounding box is constructed around the solids creates by the particles in the file. An intersection check is performed between every analyzed halo and this box. Only the lines of sight which reside in halos that pass this check are analyzed further.

2. Intersection checks are performed between every halo and solid in the catalog file.

3. For each halo, the set of intersecting solids is iterated over. For each of the halo's rings, perform an intersection check is performed between the solid and the plane which the ring is embedded within. If this check is successful, the shape corresponding to the intersection between the plane and the surface of the solid is computed.

4. The angles of the the upper and lower edges of the shape are calculated relative to the center of the halo along the corresponding plane. This identifies eactly the set of lines of sight in this ring which interect the object.

5. An intersection check is performed between the solid and these lines of sight to calculate $r_{\rm in}$ and $r_{\rm out}$.

6. The combined step function is added to the appropriate radial profile as shown in Eq. A1.

This is illustrated in Fig. 7.

The process described above has a number of inefficiencies. The most important algorithmic optimizations are described below:

- The first time step 1 is performed in a given simulation, Shellfish writes these bounding boxes to a series of header files so that they do not need to be recomputed.

- Shellfish restricts ever halo to have the rings with the same set of normal vectors. It performs step 3 by first iterating over the set of normal vectors and rotating all the solids into a coordinate system in which that normal vector is pointed in the $\hat{z}$ direction. Since this only needs to be done once across many halos, the amortized cost is small and it allows the geometric primitives needed in this step to be significantly optimized.

- For virtually all solids, it is more efficient to perform an intersection check betwen a line and the 2D shape found at the end of step 3 than it is to do an intersection check between a ray and the solid in 3D. For this reason, step 5 is performed with the former and not the latter.

[6] For the purposes of this analysis, it is assumed that performing an intersection check is also sufficient to evaluate $r_{\rm in}$ and $r_{\rm out}$. This is true for virtually all solids.

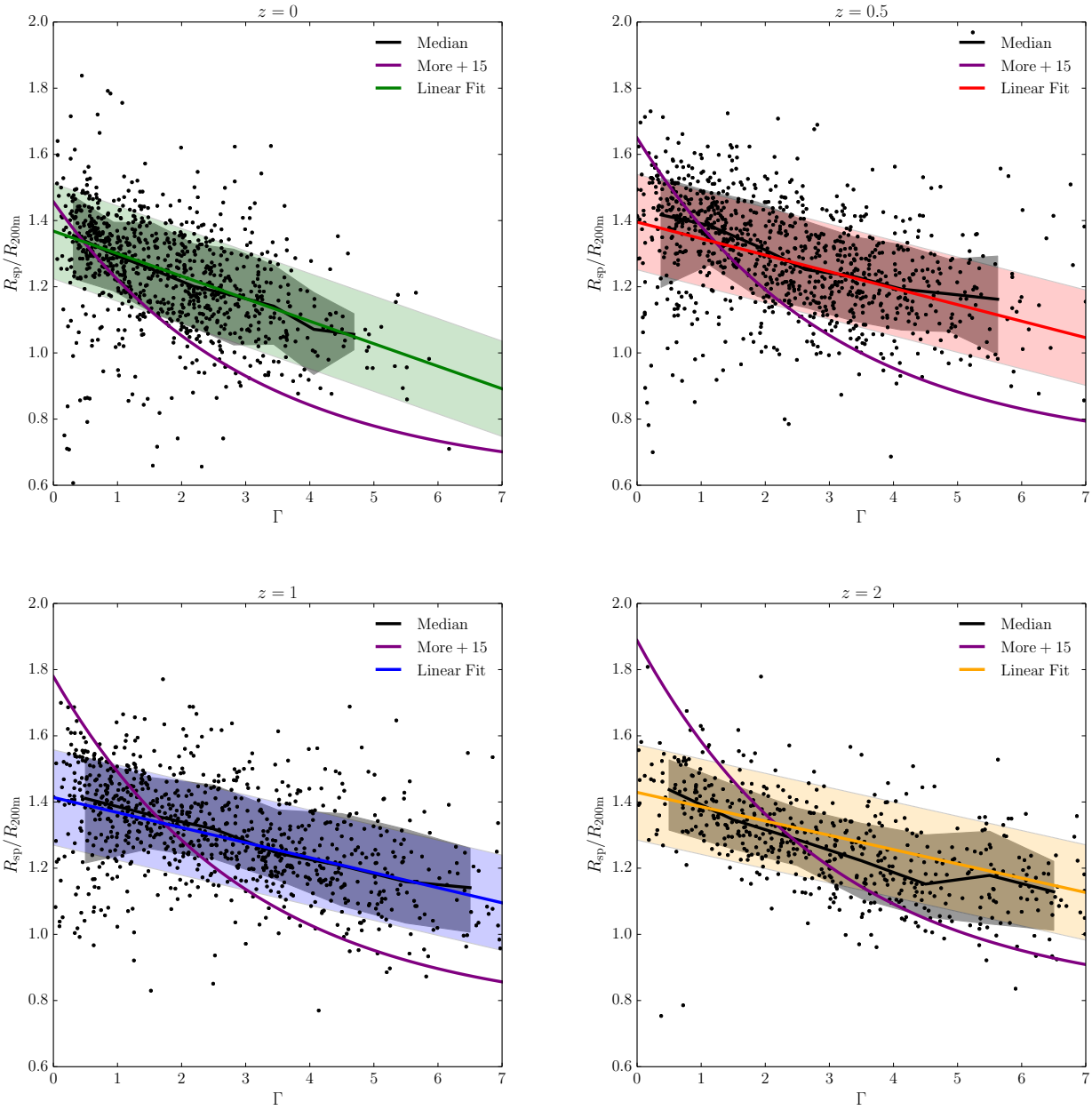

FIG. 6.— The $R_{\rm sp}/R_{\rm 200m}$ vs. Γ relation as measured by Shellfish. The points are individual halos, the black curves and gray shaded regions are the medians and the 68% envelopes of the point distributions, respectively. The colored curves and shaded regions are the peak and 1σ tails of the fitted distribution given by (**insert reference**). The purple curve is the relation given in More et al. (2015), which is found by finding the point of steepest slope of stacked profiles. The two families of curves are different in both shape and amplitude.

- If all other optimizations are performed and step 6 is implemented naively, it is the dominating cost in the procedure despite its simplicity. For this reason, instead of representing the profiles as arrays containing $\rho(r)$, we represent them as arrays containing $\mathrm{d}\rho(r)/\mathrm{d}r$. This means that every update of the profile requires modifying at most four array elements near $r_{\rm in}$ and $r_{\rm out}$. Once every solid has been looped over, the profiles are integrated to optain $\rho(r)$.

For a system with N solids, L lines of sight, I total intersection points between all solids and all lines of sight, and B radial bins per profile, a naive evaluation of Eq. A1 would require $O(NL)$ intersection checks and $O(IB)$ updates to density profiles. The algorithm we presented above performs $O(I)$ intersection checks, $O(I)$ updates to profiles, a post-processing step which performs $O(LB)$ profile accesses, and a preprocessing step that performs $O(NR)$ geometric operations, where R is the total number of rings. Since $L \ll I \ll NL$ and $1 \ll L$, this corresponds to a reduction in the number of operations by many orders of magnitude.

B. VISUALLY IDENTIFYING SPLASHBACK RADII FROM DENSITY PROFILES

(Flesh out this section eventually. Should probably move to main text.)

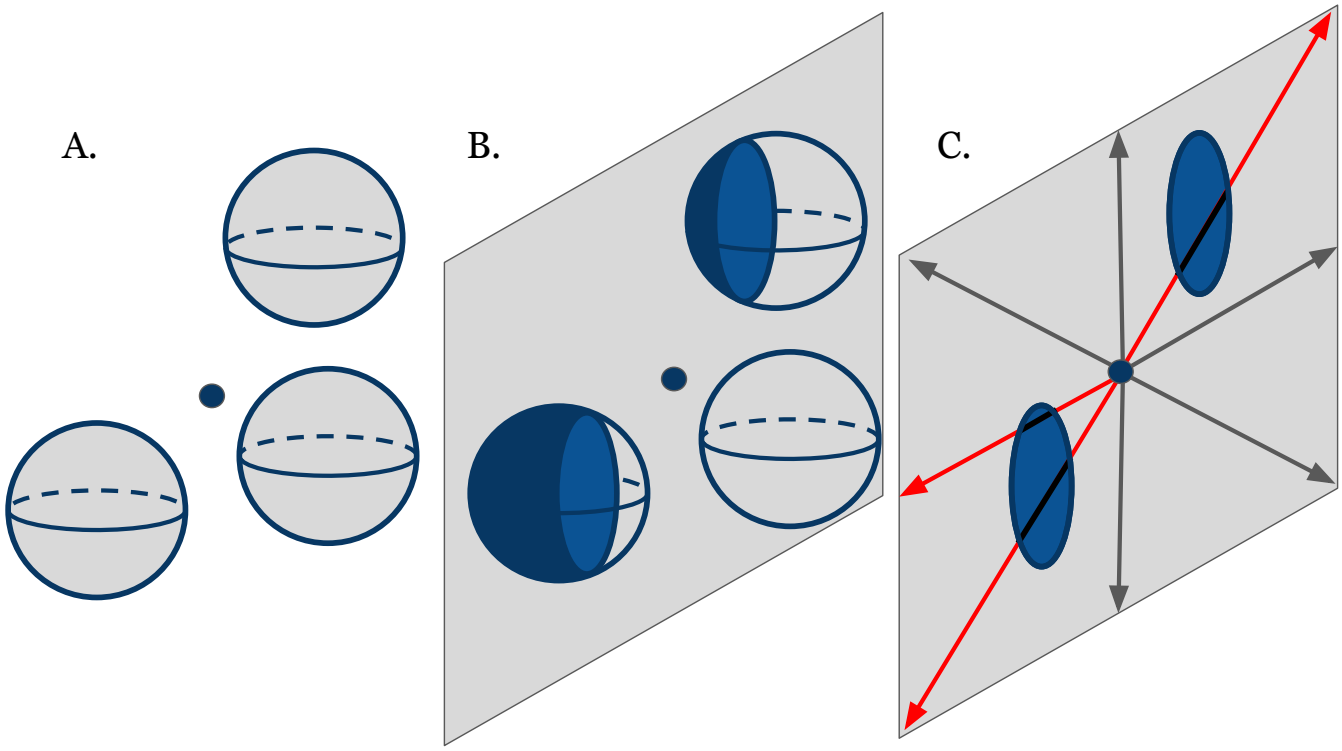

FIG. 7.— An illustration of the algorithm described in this Appendix. Panel A shows several spherical kernels oriented around the center of a halo which have successfully passed steps 1 and 2 of the algorithm. Panel B shows interseciton checks being made on a plane corresponding to a ring of line of sight rays. The top and left spheres intersect this plane while the remaining sphere does not. This corresponds to step 3 of the algorithm. Panel C shows intersection checks being performed between the 2D slices of the kernels and the lines of sight in the ring. Inspection of the angular locations of the edges of these slices shows that only the red lines of sight could intersect them, meaning that no calculations are performed on the black lines. This corresponds to steps 4 and 5 of the algorithm.

(Roughly from the most strict to least strict cut.)
(The main purpose of all of these is to rule out splashback regions which are either created or distorted by suhalos or mergers.)

- The halo is not within $R_{\rm 200m}$ of a larger halo.
- The halo much have an apparent steepening of both the density and subhalo density profiles at the same radial range.
- There must not be a "large" subhalo ($M_{\rm 200m,\ sub} > M_{\rm 200m,\ host}/15$) exactly at the start of the steepening region.
- There must not be significant subhalo presence in the steepening region.
- The slope of the steepening region must be steeper than -3.
- The concentration of the halo must be greater than 2.

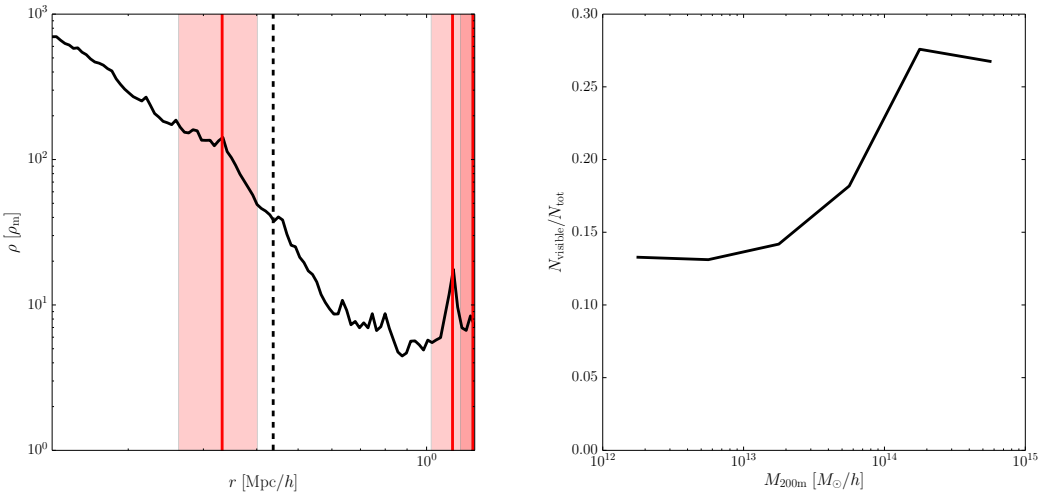

FIG. 8.— *Left:* An example profile of an $M_{\rm 200m} = 5 \times 10^{12}\ M_\odot/h$ halo which would not be included in the set of halos with visually identifiable splashback ranges. The plot show a one decade window centered around $R_{\rm 200m}$ (shown by the vertical dashed line). The vertical red lines show the location of every subhalo with $M_{\rm 200m,\ sub} > M_{\rm 200m,\ host}/15$ and the shaded regions correspond to the radial range enclosed by $R_{\rm 500c}$ for these halos. This halo would not meet the cut described in this Appendix because the apparent start of the splashback zone conicides exactly with the peak of a subhalo, making the true start of the splashback zone unclear. *Right:* The fraction of halos which pass the cuts described in this Appendix as a function of mass. The number of such halos increases with increasing mass, but even at the highest masses the majority of halos do not meet these cuts.